Effects of Zinc Precursor, Basicity and Temperature on the Aqueous Synthesis of ZnO Nanocrystals

Maroua Mrad, Bilel Chouchene and Tahar Ben Chaabane*

Unité de Recherche Synthèse et Structure de Nanomatériaux UR 11 ES 30. Faculté des Sciences de Bizerte, 7021 Jarzouna, Bizerte. Université de Carthage, Tunisia.

Received 8 November 2017, revised 13 June 2018, accepted 24 July 2018.

ABSTRACT

The effects of the zinc salt precursors, the reaction temperature and the alkaline ratio b (b = [OH-]/[Zn^{2+}]) on the aqueous synthesis of ZnO nanocrystals were investigated. Depending on the type of the zinc precursor, $Zn_5(OH)_8Cl_2{\cdot}H_2O$ or $Zn_5(OH)_8(NO_3)_2.2H_2O$ lamellar phases were obtained at room temperature (20 °C) when the alkaline ratio is lower ($0.5 \leq b \leq 1$, $6 \leq pH \leq 6.4$). When the reaction temperature increased to 95 °C, zinc hydroxide chloride monohydrate was obtained in one case whereas zinc oxide was formed in the other, and no lamellar phase of $Zn_5(OH)_8(NO_3)_2.2H_2O$ was obtained. Thermal decomposition of the two lamellar phases was carried out and mainly showed that $Zn_5(OH)_8(NO_3)_2.2H_2O$ was completely decomposed to ZnO when the annealed temperature reached ~250 °C while $Zn_5(OH)_8Cl_2{\cdot}H_2O$ was totally transformed to ZnO at about 400 °C, a higher comparative temperature that confirms the better thermal stability of the zinc hydroxide chloride monohydrate.

KEYWORDS

Oxides, ZnO, chemical synthesis, X-ray diffraction, crystal structure, luminescence.

1. Introduction

Among the various II–VI semiconductors such as ZnS, ZnSe, CdTe, CdS, etc., zinc oxide (ZnO) plays an important role in terms of chemical and physical properties. ZnO possesses remarkable characteristics, e.g. it is a wide bandgap semiconductor (3.37 eV) with a large excitonic binding energy of 60 meV. Nanostructured ZnO remains an attractive material because it has great potential for a variety of practical applications, such as in nanoscale devices, as light-emitting diodes,[1,2] magneto-optical devices,[3] ultraviolet lasers,[4,5] gas sensors,[6,7] solar cells,[8,9] photocatalysis, etc.[10,11] ZnO nanocrystals can be obtained in numerous morphological varieties related to a multitude of synthesis approaches. Particularly, various soft chemistry synthesis techniques have been developed to elaborate ZnO nanocrystals with good crystallinity and controllable shape and size, such as hydrothermal or solvothermal process,[12,13] sol-gel,[14] precipitation method,[15,16] polyol process, etc.[17,18]

In this work, we have adopted the cost competitive and simple aqueous precipitation process using low-cost precursors such as zinc nitrate or zinc chloride together with sodium or potassium hydroxide to prepare zinc oxide. Our main purpose is to evaluate the influence of the zinc precursors, the basicity and the temperature on the aqueous synthesis of ZnO. We demonstrate the important role of the alkaline ratio b (b = [OH^-]/[Zn^{2+}]) and the temperature on the ZnO wurtzite phase formation.

As far as we know, systematic investigations of the basicity, in this case medium basicity, and the temperature effects on the ZnO synthesis, especially for the lower alkaline ratios ($b \leq 2$), has rarely been studied. For instance, A.M. Pourrahimi *et al.* have prepared ZnO nanoparticles in aqueous media, from different zinc salts and sodium hydroxide, under identical conditions with a fixed alkaline ratio (b = 2.5) [19]. The NaOH solution (0.5 M) was heated to 60 °C and added to the zinc metal salt solution (0.2 M) based on nitrate, chloride, sulfate or acetate. The mixture was stirred and maintained at 60 °C for 1 h. The recuperated powders were characterized as wurtzite zinc oxide in all cases; nevertheless, the resulting nanocrystals were obtained with different morphologies that depended on the counterion type of the zinc salt.[19]

R.A. McBride *et al.* have studied the role of the zinc precursor and the temperature on the microcrystalline morphology of ZnO.[20] They prepared zinc oxide using an aqueous solution of zinc salt (0.04 M) and sodium hydroxide with a relatively higher alkaline ratio: [OH^-]/[Zn^{2+}] = 15. The authors have used two general preparative procedures; the first involves simply heating the aqueous solution to 101 °C for 8 h which then led to the formation of star-like microcrystals of the wurtzite phase. In the second method, the same reagents were stirred at room temperature for 2 h to form wulfingite ε-$Zn(OH)_2$ as an intermediate phase. When the mixture was heated to 101 °C for 24 h, ε-$Zn(OH)_2$ transformed to ZnO nanocrystals with needle shape.

L. Jiang *et al.* have reported the synthesis of ZnO crystals under hydrothermal conditions at 180 °C using zinc nitrate and sodium hydroxide with a high alkaline ratio of 20, 30 and 80.[21] All the as-synthesized products were formed with the wurtzite zinc oxide phase exhibiting flower-like morphology with sizes of 5–8 μm when the alkaline ratio was adjusted to 20. Increasing the alkaline ratio to b = 30, the same crystals morphology was obtained but with larger sizes of 10–20 μm.

It is interesting to note that increasing attention is being paid to the solution growth of ZnO nanostructures to obtain different morphologies.[22–24] Zinc oxide crystal formation involves the two processes of nucleation and growth. It is established that nucleation frequency and growth rate direct the shape and the size of ZnO crystals. The formation mechanism of the synthesized zinc oxide nanostructures in solution has been proposed and discussed by many groups.[25,28] Generally, the suggested mechanism is based on the formation of wulfingite ε-$Zn(OH)_2$ intermediate phase that transforms to ZnO wurtzite phase. Three mechanisms have been proposed:

(1) Formation of ZnO from ε-$Zn(OH)_2$ by dissolution and reprecipitation.

(2) *In situ* crystallization of ZnO from $Zn(OH)_2$ by dehydration and internal atomic arrangement.

* To whom correspondence should be addressed. E-mail: taharbch@yahoo.com

ISSN 0379-4350 Online / ©2018 South African Chemical Institute / http://saci.co.za/journal
DOI: https://doi.org/10.17159/0379-4350/2018/v71a13

(3) Direct solid-solid phase transformation which occurs in the $Zn(OH)_2$ matrix.[29]

In this paper, we mainly studied the effect of the alkaline ratio b varying it in the range 0.5–4, as well as the zinc salt precursor and the reaction temperature on the formation of the ZnO wurtzite phase and/or of intermediate phases. We noted that no ε-$Zn(OH)_2$ was formed as an intermediate species under our experimental conditions. Possible reaction processes of the formation of ZnO or of the intermediate phases are proposed and discussed.

2. Experimental

2.1. Synthesis

Zinc nitrate hexahydrate ($Zn(NO_3)_2.6H_2O$ from Sigma-Aldrich, 98 % purity), zinc chloride (ZnCl2 from Fluka, 98% purity), polyvinylpyrrolidone (PVP_{40}, average molecular weight of 40 000) and sodium hydroxide (NaOH, 98%) were used as received without additional purification. All samples were prepared in aqueous medium using twice-distilled water. We have adopted two preparative procedures; the first involves the samples (series SI) prepared at room temperature (20 °C), the second concerns the ones prepared at 95 °C (series SII).

In a typical synthesis, an appropriate quantity of zinc salt precursor (chloride or nitrate of 0.2 M) and a fixed mass of 1391 mg of PVP_{40}, used as a dispersing agent as well as stabilizer of the crystals produced, were dissolved in twice-distilled water. A given mass of NaOH base, obtained by varying the alkaline ratio b of OH^-/Zn^{2+} from 0.5 to 4, was added to the solution. A white precipitate was immediately formed in the mixture which was kept under vigorous stirring at 20 °C for 20 min (series SI). Next, the pH value of each solution was measured and noted. For the second procedure (series SII), each sample was prepared in the same way as SI but additionally heated to and maintained at 95 °C for 3 h under stirring. After cooling to room temperature, the resulting white precipitate (SI or SII) was centrifuged, washed several times with water and ethanol, and then dried in air at 60 °C for 12 h.

Once heat treatment of the samples was achieved, the powders were placed into crucible and annealed in air for 2 h at different temperatures in the range of 100–400 °C.

2.2. Characterization Techniques

The X-ray powder diffraction (XRD) patterns were recorded on a Bruker D8 Advance apparatus with Cu(K_α) radiation (λ = 1.5406 Å). XRD patterns of the recuperated powders were recorded in the scan range 2θ = 5–85 °. The average crystallite sizes were calculated from the width of the XRD peaks using the Scherrer formula.[30]

Fourier transform infrared (FT-IR) spectra were recorded on a Thermo Scientific Nicolet IR 200 spectrophotometer in the range of 400–4000 cm^{-1}.

The photoluminescence (PL) measurements were carried out at room temperature using a Perkin-Elmer spectrophotometer (LS 55) with Xenon lamp source and 320 nm excitation wavelength.

3. Results and Discussion

3.1. Structure of the Samples and Photoluminescence of ZnO

3.1.1. *Structural Study*

a) Samples Prepared at 95 °C (SII)

XRD patterns of the powders synthesized at 95 °C with different alkaline ratios are given in Fig. 1A,B).

For all the samples prepared with zinc nitrate (Fig. 1A), the XRD diffractograms are quite similar even though the alkaline ratio b was varied in the range 1–4. Interestingly, a new phase was formed at lower alkaline ratio (b = 1) for the samples synthesized with zinc chloride precursor (Fig. 1B) ; the intense diffraction peak appearing at the low diffraction angle of 11.23 ° is a typical characteristic of a layered compound having a large inter-layer spacing. This phase was identified as chloride lamellar phase (CLP) which was formed at a lower pH value (~6.3). Note that no similar layered phase was obtained for the samples prepared with zinc nitrate precursor under the same conditions. This result clearly showed that zinc chloride and zinc nitrate have different behaviour that could be related to structural characteristics of the two lamellar phases associated with each of the precursors.

The peak positions of all the XRD patterns (except Fig. 1B for b = 1) are matching well with the data reported in JCPDS Card No. 36-1451 for the wurtzite zinc oxide.[31,32] The XRD diagrams (Fig. 1A,B) reveal well-crystallized ZnO powder; the peak broadening indicated the nature of the small nanocrystals. Crystallite sizes of ZnO were estimated following the well-known Scherrer equation: $L = 0.9\lambda/(\beta\cos\theta)$ where L represents crystallite size (Å),

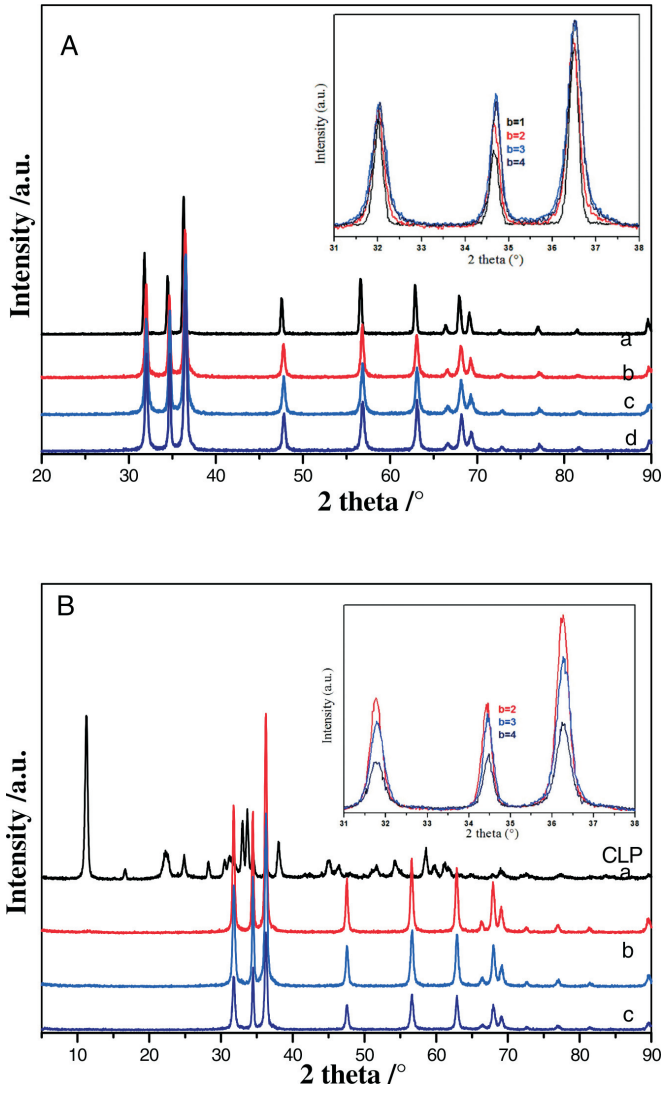

Figure 1 X-ray diffraction patterns of samples (SII) prepared at 95 °C : (**A**) synthesized with zinc nitrate : a (b= 1), b (b= 2) , c (b= 3), d (b=4) ; (**B**) synthesized with zinc chloride : CLP (chloride lamellar phase) a (b= 2), b (b= 3) , c (b= 4). The insets (A and B) : zoom of the ZnO diffraction peaks in the 2θ range 30–40 °.

λ is the wavelength of Cu(Kα) radiation (Å) and β is the corrected full width at half maximum (FWHM) of the diffraction peak.[30]

The average crystallite sizes of ZnO were calculated by considering the first three peaks (100), (002) and (101) and are found to decrease when the alkaline ratio was increased; 48 nm and 28–30 nm for b=1 and b=4, respectively, for both ZN samples prepared with $Zn(NO_3)_2.6H_2O$ and ZC ones synthesized using $ZnCl_2$ salt (Table 1).

Note that the effect of the pH medium on ZnO crystallites sizes is not yet well clearly understood and contradictory results could be found in the literature. For instance, S.S. Alias *et al.* have reported results which are in accordance with ours.[33] The authors prepared ZnO nanocrystals in methanol as solvent at 25 °C under stirring for 2 h using $Zn(CH_3CO_2)_2{\cdot}2H_2O$ (0.2 M) and NaOH solution (1M) as reactants in the pH range 6–13. They found that further increase in OH^- concentration in ZnO (pH 10 and 11) reduced the crystallite sizes because ZnO can be dissolved when it reacted with excessive OH^- ions.

On the other hand, M. J. Chithra *et al.* have synthesized ZnO nanoparticles by chemical precipitation in ethanol as solvent at 30 °C using zinc acetate (0.2 M) and NaOH. The authors have reported an opposite result; they have noted an increase in the crystallite sizes when the pH values increase, the calculated sizes were 13.8, 18.0, 24.7 and 33 nm for the samples obtained at pH values of 6, 8, 12 and 13, respectively.[34]

b) Samples Prepared at 20 °C (SI)

Powder X-ray diffraction patterns of as-prepared samples are shown in Fig. 2A,B). For lower alkaline ratios (b= 0.5; 1), pure layered hydroxide zinc salts were formed: nitrate lamellar phase (NLP) was obtained applying $Zn(NO_3)_2.6H_2O$ as precursor and chloride lamellar phase (CLP) was formed when $ZnCl_2$ was used. All the corresponding XRD peaks of NLP and CLP (Fig. 2, b=0.5 or 1 (Fig. 2A,B)) can be well indexed to monoclinic $Zn_5(OH)_8(NO_3)_2.2H_2O$ phase and hexagonal $Zn_5(OH)_8Cl_2.H_2O$ phase, respectively, and neither product could be detected in each other. It is worth noting that no wulfingite ε-$Zn(OH)_2$ phase was detected in all samples (Table 1).

Increasing the alkaline ratio b to 2 led to the coexistence of ZnO and $Zn_5(OH)_8(NO_3)_2.2H_2O$ phase (Fig. 2A, b = 2) or ZnO and $Zn_5(OH)_8Cl_2.H_2O$ phase (Fig. 2B, b = 2). Further increasing the alkaline ratio to b ≥ 3, only ZnO is formed and the lamellar phases (NLP and CLP) disappear. This indicates that the formation reaction of zinc oxide is highly promoted under strongly basic conditions (Table 1) and then, the ZnO wurtzite phase is formed independent of the nature of the zinc precursor.

Furthermore, it is interesting to report that using KOH as a second base instead of NaOH led to identical results for the two series (SI and SII) indicating that the counter-ion of the strong base MOH (M= Na or K) does not affect the products of the different reactions.

Based on this observed results, we suggest a possible reaction processes for the formation of ZnO and/or lamellar compounds as follows.

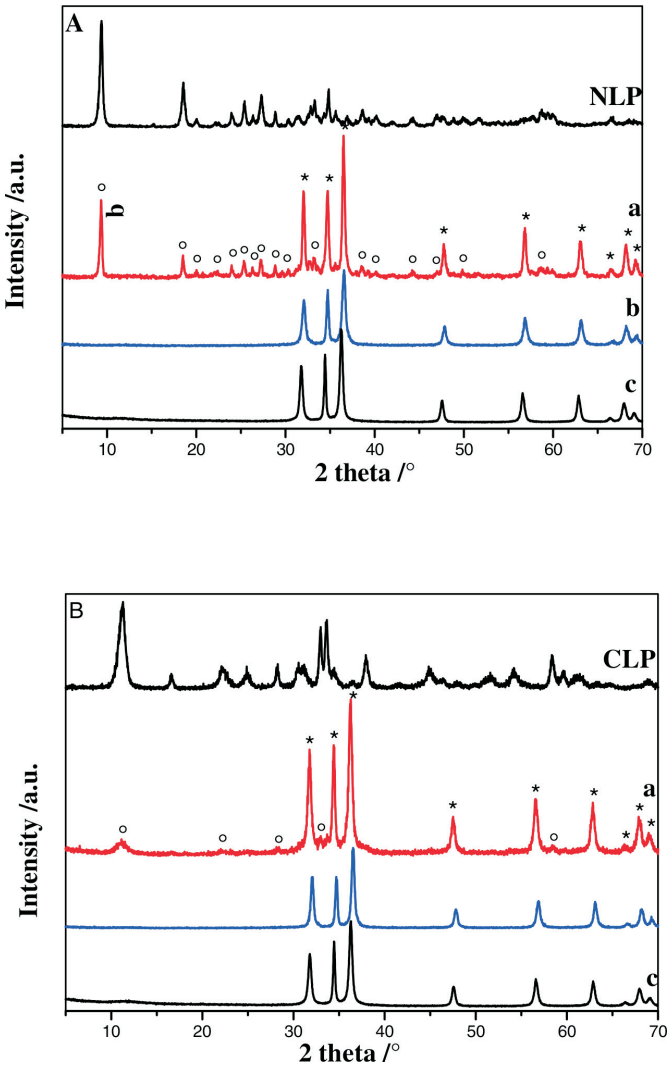

Figure 2 X-ray diffraction patterns of samples prepared at 20 °C: (**A**) synthesized with zinc nitrate: NLP (Nitrate Lamellar Phase for b= 0.5 or b =1) a (b= 2), b (b= 3), c (b= 4) ; (°) peaks of NLP , (*) peaks of ZnO wurtzite phase. (**B**) synthesized with zinc chloride: CLP (chloride lamellar phase for b= 0.5 or b =1) a (b= 2), b (b= 3), c (b=4). (°) peaks of CLP, (*) peaks of ZnO.

Table 1 Phase composition of samples (SI and SII) and calculated crystallite sizes of ZnO (SII).

Sample *	Alkaline ratio; pH	Phase composition (SI) prepared at 20 °C	Phase composition (SII) prepared at 95 °C	(SII) average crystallite size /nm
ZN0.5	0.5; 6.1	$Zn_5(OH)_8(NO_3)_2.2H_2O$	–	–
ZN1	1; 6.4	$Zn_5(OH)_8(NO_3)_2.2H_2O$	ZnO	48
ZN2	2; 9.9	$Zn_5(OH)_8(NO_3)_2.2H_2O$ + ZnO	ZnO	34
ZN3	3; 13	ZnO	ZnO	28
ZN4	4; 13.3	ZnO	ZnO	30
ZC0.5	0.5; 6.1	$Zn_5(OH)_8Cl_2.H_2O$	–	–
ZC1	1; 6.3	$Zn_5(OH)_8Cl_2.H_2O$	$Zn_5(OH)_8Cl_2.H_2O$	–
ZC2	2; 10.9	$Zn_5(OH)_8Cl_2.H_2O$+ ZnO ZnO	ZnO	31
ZC3	3; 13.1	ZnO	ZnO	28
ZC4	4; 13.4	ZnO	ZnO	28

* ZN prepared using $Zn(NO_3)_2.6H_2O$; ZC prepared using $ZnCl_2$.

b=1 ([OH⁻]/[Zn²⁺] =1)

$(Zn^{2+} + 2\,Cl^-) + (M^+ + OH^-) + 1/8\,H_2O \longrightarrow$
$1/8\,Zn_5(OH)_8Cl_2.H_2O + 3/8\,(Zn^{2+} + 2\,Cl^-) + (M^+ + Cl^-)$
$(Zn^{2+} + 2\,NO_3^-) + (M^+ + OH^-) + 1/4\,H_2O \longrightarrow$
$1/8\,Zn_5(OH)_8(NO_3)_2.2H_2O + 3/8\,(Zn^{2+} + 2\,NO_3^-) + (M^+ + NO_3^-)$

b=2 ([OH⁻]/[Zn²⁺] =2)

$(Zn^{2+} + 2\,Cl^-) + \mathbf{2}\,(M^+ + OH^-) \longrightarrow$
$1/8\,Zn_5(OH)_8Cl_2.H_2O + 3/8\,ZnO + 1/4\,(M^+ + OH^-) + 7/4(M^+ + Cl^-) + 1/4\,H_2O.$
$(Zn^{2+} + 2\,NO_3^-) + \mathbf{2}\,(M^+ + OH^-) \longrightarrow$
$1/8\,Zn_5(OH)_8(NO_3)_2.2H_2O + 3/8\,ZnO + 1/4\,(M^+ + OH^-) + 7/4(M^+ + NO_3^-) + 1/8\,H_2O.$

b= n ≥ 3 ([OH⁻]/[Zn²⁺] ≥ 3)

$(Zn^{2+} + 2\,X^-) + \mathbf{n}\,(M^+ + OH^-) \longrightarrow$
$ZnO + 2\,(M^+ + X^-) + (n-2)\,(M^+ + OH^-) + H_2O$ with $X^- = NO_3^-$ or Cl^-

c) Structure of Lamellar Phases

The chloride lamellar phase $Zn_5(OH)_8Cl_2.H_2O$ (CLP) crystallizes in the space group R-3m with the following hexagonal cell parameters: a= b = 6.3412 Å , c = 23.650 Å , $\alpha = \beta = 90$ °, $\gamma = 120$ °.[35] A projection of the atomic arrangement of CLP, along the b axis, is given in Fig. 3.

The CLP structure consists of infinite layers perpendicular to the c direction and separated by 7.88 Å (c/3). These sheets are formed by interconnected $Zn(OH)_6$ octahedra. The water molecules and $Zn(OH)_3Cl$ tetrahedra are located between these sheets.

The nitrate lamellar phase (NLP), $Zn_5(OH)_8(NO_3)_2.2H_2O$, belongs to the space group C2/m with a monoclinic cell: $a = 19.48, b = 6.238, c = 5.517$A °, $\beta = 83.28$° (PDF card No. 72–0627).[36]

A projection of the NLP structure is illustrated in Fig. 4. It shows infinite parallel layers of $Zn(OH)_6$ octahedra. The zinc tetrahedra $Zn(OH)_3(O_{water})$ and nitrate ions are inserted between theses sheets which are related by weak hydrogen bonds. The inter-layer distance is about 9.74 Å corresponding to a/2. Compared to the CLP structure, the NLP compound exhibits a longer distance between the sheets and its nitrate units are not involved in the coordination sphere of the zinc cation unlike CLP compound where the chloride ion is actually connected to zinc tetrahedron ($Zn(OH)_3Cl$). Based on these observations, $Zn_5(OH)_8Cl_2.H_2O$ solid may have a more rigid framework and thus we can expect a higher thermal stability for CLP. This is why, unlike $Zn_5(OH)_8Cl_2.H_2O$, the NLP phase was not obtained *via* the second synthesis procedure realized at 95 °C (series SII, b=1) because of its low stability: $Zn_5(OH)_8(NO_3)_2.2H_2O$ may decompose at 95 °C to produce ZnO.

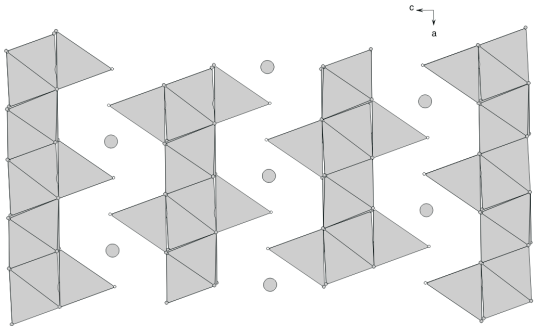

Figure 3 A projection of $Zn_5(OH)_8Cl_2.H_2O$ structure (grey circles: oxygen atoms of water molecules, hatched polyhedra: $Zn(OH)_6$ octahedra, simple polyhedra: $Zn(OH)_3Cl$ tetrahedra)

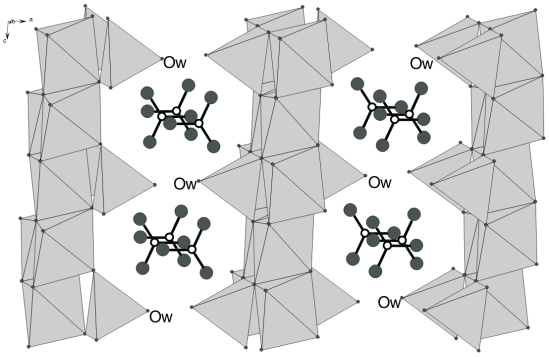

Figure 4 A projection of $Zn_5(OH)_8(NO_3)_2.2H_2O$ structure (dark circles: oxygen atoms of nitrate units, empty circles: nitrogen atoms, hatched polyhedra: $Zn(OH)_6$ octahedra, simple polyhedra: $Zn(OH)_3(O_{water})$ tetrahedra, Ow: oxygen atom of water molecule).

3.1.2. *Photoluminescence Analysis of ZnO*

ZN3(SII) and ZC3(SII) samples prepared with different zinc salts and corresponding to hexagonal zinc oxide were selected for the photoluminescence (PL) analysis. Their room temperature PL spectra are given in Fig. 5.

Generally, ZnO wurtzite photoluminescence spectrum typically exhibits emission bands in the near UV and in the visible range.[37,38] The UV emission (360–380 nm) is associated with the radiative recombination of an electron from the conduction band with a hole located in the valence band (band-edge emission) or in a trap near the valence band (near-band-edge emission). The visible luminescence of ZnO contains violet–blue (390–480 nm), green (500–520 nm), yellow–orange (560–600 nm) and red (650–670 nm) bands. The origin of the visible luminescence is frequently related to numerous ZnO defects such as oxygen vacancies (V_O), zinc vacancies (V_{Zn}), oxygen intersticials

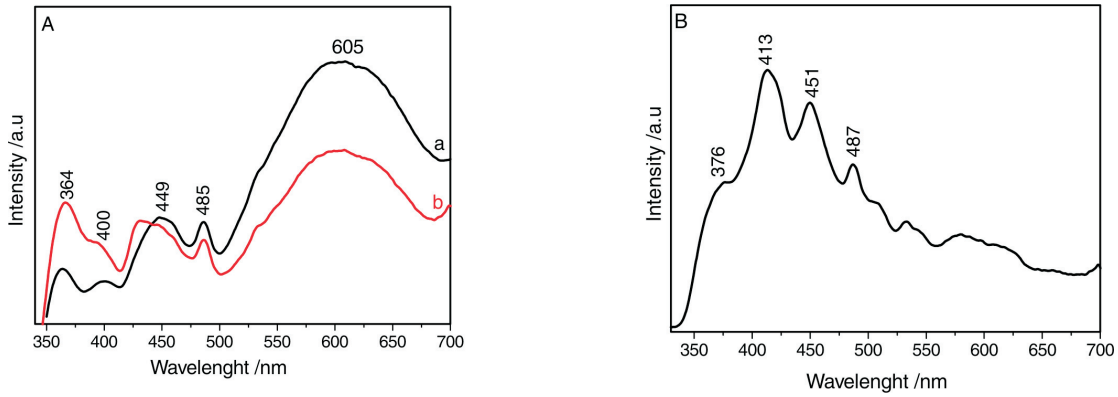

Figure 5 Room temperature photoluminescence spectra of ZnO (λ_{exc} = 320 nm). (**A**): (a) for ZN3(SII) and (b) for ZC3(SII) ; (**B**): ZN3(SII) annealed at 300 °C for 2 h.

(Oi), zinc intersticials (Zni), antisite oxygen (O_{Zn}) and extrinsic impurities.[39,40]

ZN3(SII) and ZC3(SII) exhibit comparable luminescence spectra not only in the UV domain (364 nm) but also in the visible region characterized by a dominant large band in 500–690 nm, centred at ~ 605 nm (Fig. 5A). Nevertheless, ZC3(SII) presents a stronger UV band at 364 nm ascribed to the free exciton recombination but emits less intense visible bands. Generally, ZnO nanostructures with relatively small size and abundant structural defects present strong emissions in the visible region.[40,41] Comparatively, the intense UV emission band joined to the weak visible emission bands may give evidence for the better crystallinity of the ZnO prepared with the zinc chloride salt. Therefore, ZnO nanocrystals of ZN3(SII) sample are formed with more intrinsic defects that are, manifestly, dependent on the nature of the zinc salt precursor.

In the purpose to improve the ZN3(SII) cristallinity, this sample was annealed at 300 °C for 2 h and then its PL spectrum was recorded (Fig. 5B). Interestingly, the thermally treated nanocrystals show that the UV emission band (~376 nm) becomes more intense and the large visible emission in the range 500–690 nm becomes remarkably reduced.

It was thus shown that the annealing process improved the ZN3(SII) crystallinity and minimized the number of its structural defects.[42]

3.2. Thermal Decomposition of Lamellar Phases

In order to investigate the thermal stabilities of the tow lamellar intermediate phases, diffraction patterns of annealed CLP and NLP samples at various temperatures are recorded (Figs. 6 and 7). For each phase, we considered only one sample that underwent successive thermal treatments at different temperatures.

3.2.1. *Chloride Lamellar Phase (CLP)*

The CLP diffractogram of the sample heated at 100 °C and the non-annealed one (Fig. 6) are identical and no structural change was observed. When the annealing temperature was increased to 250 °C, the CLP ($Zn_5(OH)_8Cl2.H_2O$) was partially decomposed and three phases were obtained, namely, CLP, ZnO wurtzite and β-Zn(OH)Cl which was identified by its most intense diffraction peak appearing at 15.7 ° corresponding to the interreticular distance d(0 0 2) = 0.565 nm (Fig. 6, b).[35]

The same previous three phases were still detected when the sample was annealed at 300 °C but we noticed a narrowing of the CLP diffraction peaks widths with a very weak shift towards the higher 2θ angles (Fig. 6, c). Further increasing the annealing temperature to 350 °C led to the disappearance of β-Zn(OH)Cl and the presence of a mixture of the two previous phases that appear with a remarkable disproportionate amount; a very minor amount of the CLP phase and a major amount of the ZnO phase (Fig. 6, d).

The XRD pattern in Fig. 6 (e) shows that only the diffraction peaks of ZnO wurtzite are detected after annealing at 400 °C for 2 h suggesting the complete decomposition of $Zn_5(OH)_8Cl_2{\cdot}H_2O$.

Based on these observed results, it is possible to propose the following reaction processes to account for the thermal decomposition of $Zn_5(OH)_8Cl_2{\cdot}H_2O$ lamellar phase :

$$Zn_5(OH)_8Cl_2{\cdot}H_2O \xrightleftharpoons{(20\,^\circ C - 100\,^\circ C)\,(2\,h)} Zn_5(OH)_8Cl_2{\cdot}H_2O.$$

$$Zn_5(OH)_8Cl_2{\cdot}H_2O \xrightleftharpoons{(250\,^\circ C - 300\,^\circ C)\,(2\,h)} 2\,Zn(OH)Cl + 3\,ZnO + 4\,H_2O_{(g)}$$
$$\xrightleftharpoons{(350\,^\circ C)\,(2\,h)} 5\,ZnO + 2\,HCl_{(g)} + 4H_2O_{(g)} \xrightarrow{(400\,^\circ C)\,(2\,h)} 5\,ZnO + 2\,HCl_{(g)} + 4H_2O_{(g)}.$$

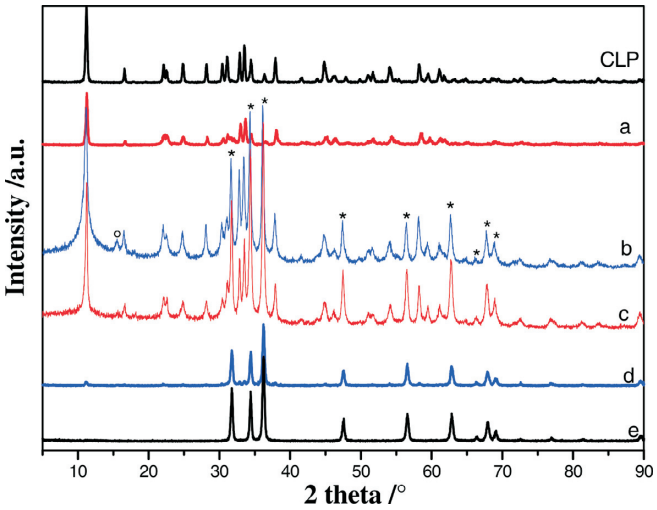

Figure 6 XRD powder patterns of chloride lamellar phase (CLP) annealed for 2 h at different temperatures: CLP at room temperature, a (100 °C), b (250 °C), c (300 °C), d (350 °C), e (400 °C); (°) peak of β-Zn(OH)Cl , (*) peaks of ZnO wurtzite phase.

3.2.2. *Nitrate Lamellar Phase (NLP)*

The X-ray powders patterns of NLP sample annealed for 2 h at various temperatures are given in Fig. 7. The sample heated at 100 °C and the non-annealed one have the same diffraction pattern corresponding to $Zn_5(OH)_8(NO_3)_2.2H_2O$ (NLP). Increasing the temperature to 150 °C (Fig. 7, b) shows the complete disappearance of the NLP phase that decomposes into a mixture of ZnO and monoclinic $Zn_3(OH)_4(NO_3)_2$ (S.G : P21/C) having a most intense peak appearing at 12.9 ° and corresponding to $d_{(100)}$.[43]

The XRD patterns of the sample heated at 200 °C and 250 °C (Fig. 7, c and d) show the disappearance of $Zn_3(OH)_4(NO_3)_2$ and the formation of wurtzite zinc oxide which exhibits intense and well-defined diffraction peaks indicating the improved crystallization of ZnO nanocrystals after annealing at these temperatures.

In view of these observations and based on some previous published works,[44,45] we can propose the decomposition reactions as follows:

$$Zn_5(OH)_8(NO_3)_2.2H_2O \xrightleftharpoons{(20\text{–}100\,^\circ C)\,(2\,h)} Zn_5(OH)_8(NO_3)_2.2H_2O.$$

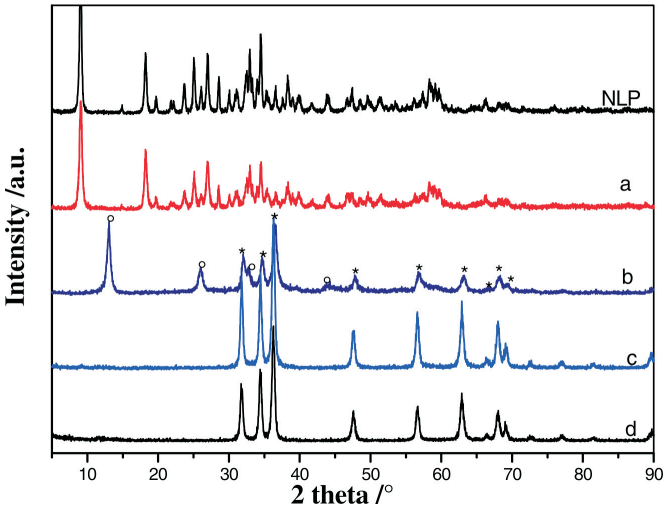

Figure 7 XRD powder patterns of nitrate lamellar phase (NLP) heated for 2 h at different temperatures: NLP at room temperature, a (100 °C), b (150 °C), c (200 °C), d (250 °C) ; (°) peaks of $Zn_3(OH)_4(NO_3)_2$, (*) peaks of ZnO wurtzite phase.

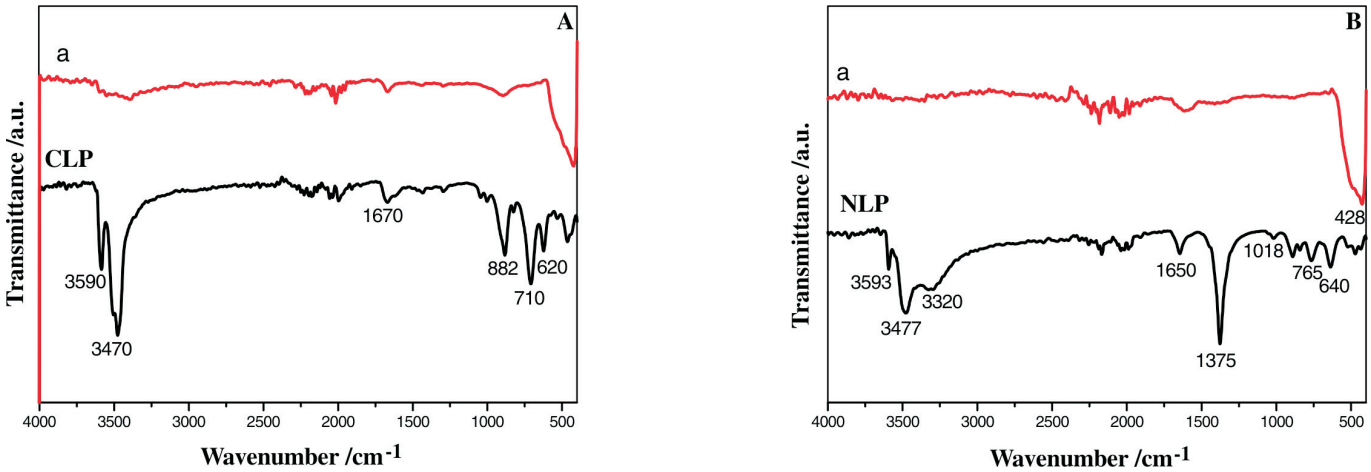

Figure 8 FTIR spectra of lamellar phases: (**A**) CLP: at room temperature, (a) CLP after annealing up to 400 °C. (**B**) NLP: at room temperature, (a) NLP after annealing up to 250 °C.

$Zn_5(OH)_8(NO_3)_2.2H_2O \xrightarrow{(150\ °C)\ (2\ h)} Zn_3(OH)_4(NO_3)_2 + 2\ ZnO +$
$4\ H_2O_{(g)} \xrightarrow{(200–250\ °C)\ (2\ h)} 5\ ZnO + 5\ H_2O_{(g)} + 2\ HNO_{3(g)}.$

It can be seen from this qualitative thermal study of the intermediate lamellar phases that the CLP presents the highest thermal stability. In fact, $Zn_5(OH)_8Cl_2{\cdot}H_2O$ is completely decomposed into ZnO only when the annealing temperature exceeds 350 °C. On the other hand, $Zn_5(OH)_8(NO_3)_2.2H_2O$ (NLP) is totally transformed, at only 150 °C, into ZnO and $Zn_3(OH)_4(NO_3)_2$ which is wholly decomposed into ZnO when the temperature reaches 200–250 °C.

These results are in good accordance with the structural characteristics of the lamellar compounds and mainly explain why the zinc salt precursors lead to different reaction products when the synthesis process was realized at 95 °C using lower alkaline ratio (SII (b = 1)).

3.3. FT-IR Spectroscopy Analysis

FTIR spectra (Fig. 8) of the lamellar phases were recorded and analyzed. They are also in good accordance with the structural characteristics of the two compounds, not only for the no annealed samples but also for those heated up to the highest annealing temperature; 400 °C for CLP and 250 °C for NLP. Thus, the infrared spectrum of $Zn_5(OH)_8Cl_2{\cdot}H_2O$ (Fig. 8A) contains bands in the range 3600–3400 cm^{-1} corresponding to the stretching vibrations of OH groups; the sharp band at 3590 cm^{-1} may be assigned to the vibrations of hydroxyl units and the strong one at around 3470 cm^{-1} can be ascribed to the OH stretching vibrations of the water molecules, the medium intense band at 1670 cm^{-1} is due to the bending vibrations of the H_2O molecules.[46] The intense bands at 882 and 710 cm^{-1} are due to stretching vibration modes of Zn-Cl units and the weak and sharp band at 620 cm^{-1} is assigned to the δ-mode of the O–H groups.[47–49] The CLP sample annealed up to 400 °C presents a typical infrared spectrum (Fig. 8A, a) of ZnO wurtzite phase identifiable by its characteristic strong band located at about 430 cm^{-1}.

The FTIR spectrum of $Zn_5(OH)_8(NO_3)_2.2H_2O$ (Fig. 8B) mainly contains the specific IR frequencies of the nitrate groups and the hydroxyl units. The three bands on the higher frequency side of the spectrum located at 3593, 3477 and 3320 cm^{-1} are attributed to the OH stretching vibrations of the layer hydroxyls and the water molecules; the weak band at around 1650 cm^{-1} is ascribed to the bending vibrations of H_2O species. The strong sharp band at 1375 cm^{-1}, the weak ones at 840 and 765 cm^{-1} and the very weak peak at about 1018 cm^{-1} are due to nitrate groups and correspond to their asymmetric stretch (ν_3), the asymmetric (ν_2) and symmetric (ν_4) deformations and symmetric stretch (ν_1), respectively.[45,48] Finally the weak peak at around 640 cm^{-1} can be assigned to δ(Zn-OH) bending mode.[49]

The infrared spectrum (Fig. 8B, a) of NLP annealed up to only 250 °C shows the intense band located at about 428 cm^{-1} that unambiguously corresponds to Zn-O bond vibration of the zinc oxide wurtzite phase.[50]

In view of these spectroscopic analyses, it is interesting to note that the obtained results are in good agreement with those of the thermal decomposition study and once again confirm the lower stability of NLP compared to CLP.

4. Conclusion

Using the aqueous precipitation method, we have principally demonstrated the important effect of the zinc precursor nature to condition the reaction products; zinc oxide or lamellar phases. In a similar way, the role of the reaction temperature and the basicity on the ZnO nanocrystals synthesis has been demonstrated.

When the alkaline ratio b = [OH-]/[Zn^{2+}] is lower ($0.5 \leq b \leq 1$; $6 \leq pH \leq 6.5$), $ZnCl_2$ and $Zn(NO_3)_2.6H_2O$ precursors present different behaviour and lead to distinct reaction products not only at room temperature suitable for the formation, respectively, of $Zn_5(OH)_8Cl_2{\cdot}H_2O$ (CLP) and $Zn_5(OH)_8(NO_3)_2.2H_2O$ (NLP) lamellar phases, but also at 95 °C to obtain ZnO wurtzite or $Zn_5(OH)_8Cl_2{\cdot}H_2O$ which exhibits a better thermal stability compared to NLP.

Increasing the alkaline ratio ($2 \leq b \leq 4$) leads only to ZnO formation regardless of the zinc salt precursor and the reaction temperature (20 °C or 95 °C).

In view of these results, we envisage to extend the present study to investigate the effect of the previous synthesis parameters on the size and the morphology transformation of the obtained nanocrystals for both ZnO and intermediate phases.

Acknowledgements

The authors are very thankful to Professor K. Horchani (Laboratoire de Physico-Chimie des Matériaux Minéraux et leurs Applications, Technopole de Borj Cedria, Soliman, Tunisia) for her help in acquiring the photoluminescence data.

§ORCID iD

T. B. Chaabane: orcid.org/0000-0002-0402-0450

References

1 S.J. Pearton and F. Ren , Advances in ZnO-based materials for light emitting diodes, *Curr. Opin. Chem. Eng.,* 2014, **3**, 51–55.

2 H. Dae-Kue, O. Min-Suk, L. Jae-Hong and P. Seong-Ju, ZnO thin films and light-emitting diodes, *J. Phys. D: Appl. Phys.*, 2007, **40**, R387.

3 K. Ando, H. Saito, Z. Jin, T. Fukumura, M. Kawasaki, Y. Matsumoto and H. Koinuma, Large magneto-optical effect in an oxide diluted magnetic semiconductor Zn1-xCoxO, *Appl. Phys. Lett*, 2001, **78**, 2700–2702.

4 M.H. Huang, S. Mao, H. Feick, H.Q. Yan, Y.Y. Wu, H. Kind, E. Weber, R. Russo and P.D. Yang, Room-temperature ultraviolet nanowire nanolasers, *Science,* 2001, **292**, 1897–1899.

5 K. Govender, D.S. Boyle, P. O'Brien, D. Binks, D. West and D. Coleman, Room temperature lasing observed from ZnO nanocolumns grown by aqueous solution deposition, *Adv. Mater.,* 2002, **14**, 1221–1224.

6 L. Wang, Y. Kang, X. Liu, S. Zhang, W. Huang and S. Wang, ZnO nanorod gas sensor for ethanol detection, *Sens. Act. B: Chem.,* 2012, **162**, 237–243.

7 P.H. Yeh, Z. Li and Z.L. Wang, Schottky-gated probe-free ZnO nanowire biosensor, *Adv. Mater.,* 2009, **21**, 4975–4978.

8 J. Huang, Z. Yin and Q. Zheng, Applications of ZnO in organic and hybrid solar cells, *Energy Environ. Sci,* 2011, **4**, 3861–3877.

9 B. Weintraub, Y.G. Wei and Z.L. Wang, Optical fiber/nanowire hybrid structures for efficient three-dimensional dye-sensitized solar cells, *Angew. Chem. Int. Ed.*, 2009, **48**, 8981–8985.

10 B. Chouchene, T.B. Chaabane, L. Balan, E. Girot, K. Mozet, G. Medjahdi and R. Schneider, High performance Ce-doped ZnO nanorods for sunlight-driven photocatalysis, *Beilstein J. Nanotechnol.,* 2016, **7**, 1338–1349.

11 A. Osman and A. Yüksel Controlled modulation of 1D ZnO nano/micro structures: Evaluation of the various effects on the photocatalytic activity, *J. Phys. Chem. Solids,* 2017, **108**, 88–97.

12 B. Baruwati, D.K. Kumar and S.V. Manorama, Hydrothermal synthesis of highly crystalline ZnO nanoparticles: a competitive sensor for LPG and EtOH, *Sens. Act. B: Chem.,* 2006, **119**, 676–682.

13 B. Chouchene, T.B. Chaabane, K. Mozet, E. Girot, S. Corbel, L. Balan, G. Medjahdi and R. Schneider, Porous Al-doped ZnO rods with selective adsorption properties, *Appl. Surf. Sci.,* 2017, **40**, 102–110.

14 J. Lee, A.J. Eastealb, U. Pal and D. Bhattacharyya, Evolution of ZnO nanostructures in sol–gel synthesis, *Curr. Appl. Phys.,* 2009, **9**, 792–796.

15 D. Raoufi, Synthesis and microstructural properties of ZnO nanoparticles prepared by precipitation method, *Ren. Energy,* 2013, **50**, 932–937.

16 Y. Wang , C. Zhang, S. Bi and G. Luo, Preparation of ZnO nanoparticles using the direct precipitation method in a membrane dispersion micro-structured reactor, *Powder Technol.* 2010, **202**, 130–136.

17 B. Chouchene, K. Horchani-Naifer and T.B. Chaabane, Effect of the solvent on the morphology and the size of ZnO nanoparticles synthesized in polyol medium, *Rev. Roum. Chim.,* 2016, **61**, 857–862.

18 A. Mezni, F. Kouki, S. Romdhane, B. Warot-Fonrose, S. Joulié, A. Mlayah and L.S. Smiri, Facile synthesis of ZnO nanocrystals in polyol, *Mater. Lett.,* 2012, **86**, 153–156.

19 A.M. Pourrahimi, D. Liu, L.K.H. Pallon, R.L. Andersson, A.M. Abad, J.M. Lagarón, M.S. Hedenqvist, V. Ström, U.W. Geddea and R.T. Olsson, Water-based synthesis and cleaning methods for high purity ZnO nanoparticles – comparing acetate, chloride, sulphate and nitrate zinc salt precursors, *RSC Adv.,* 2014, **4**, 35568–35577.

20 R.A. McBride, J.M. Kelly and D.E. McCormack, Growth of well-defined ZnO microparticles by hydroxide ion hydrolysis of zinc salts, *J. Mater. Chem.,* 2003, **13**, 1–7.

21 L. Jiang, G. Li, Q. Ji and H. Peng, Morphological control of flower-like ZnO nanostructures, *Mat. Lett.,* 2007, **61**, 1964–1967.

22 Y. Khan, S.K. Durrani, M. Mehmood, J. Ahmad, M.R. Khan and S. Firdous, Low temperature synthesis of fluorescent ZnO nanoparticles, *Appl. Surf. Sci.,* 2010, **257**, 1756–1761.

23 F. Demoisson, R. Piolet and F. Bernard, Hydrothermal synthesis of ZnO crystals from Zn(OH)2 metastable phases at room to supercritical conditions, *Cryst. Growth Des.,* 2014, **14**, 5388-5396.

24 P. Li, H. Liu, B. Lu and Y. Wei, Formation mechanism of 1D ZnO nanowhiskers in aqueous solution, *J. Phys. Chem. C,* 2010, **114**, 21132–21137.

25 J. Wang and L. Xiang, Formation of ZnO rods with varying diameters from ε-Zn(OH)2, *J. Cryst. Growth,* 2014, **401**, 279–284.

26 L. Guo, Y. L. Ji and H. Xu, Regularly shaped, single-crystalline ZnO nanorods with Wurtzite structure, *J. Am. Chem. Soc.,* 2002, **124**, 14864–14865.

27 J. Xie, P. Li, Y. Li, Y. Wang and Y. Wei, Morphology control of ZnO particles via aqueous solution route at low temperature, *Mater. Chem. Phys.,* 2009, **114**, 943–947.

28 A. Kołodziejczak-Radzimska and T. Jesionowski, Zinc oxide—From synthesis to application: a review, *Mater.,* 2014, **7**, 2833–2881.

29 M. Wang, Y. Zhou, Y. Zhang, S.H. Hahn and E.J. Kim, From Zn(OH)2 to ZnO: a study on the mechanism of phase transformation, *Cryst. Eng. Comm.,* 2011, **13**, 6024–6026.

30 W. Mao-Hua, F. Zhou and B. Zhang, Synthesis and characterization of low-dimensional ZnO nanocrystals in an aqueous solution, *J. Alloy. Comp.,* 2013, **581**, 308–312.

31 H.F. McMurdie, M.C. Morris, E.H. Evans, B. Paretzkin, W. Wong-Ng, L. Ettlinger and C.R. Hubbard, Standard X-ray diffraction powder patterns from the JCPDS research associateship, *Powder Diffr.,* 1986, **1**, 64–77.

32 F. Xu, P. Zhang, A. Navrotsky, Y. Zhong-Yong, R. Tie-Zhen, M. Halasa and S. Bao-Lian, Hierarchically assembled porous ZnO nanoparticles: synthesis, surface energy, and photocatalytic activity, *Chem. Mater.,* 2007, **19**, 5680–5686.

33 S.S. Alias, A.B. Ismail and A.A. Mohamad, Effect of pH on ZnO nanoparticle properties synthesized by sol-gel centrifugation, *J. Alloy. Comp.,* 2010, **499**, 231–237.

34 M.J. Chithra, M. Sathya and K. Pushpanathan, Effect of pH on crystal size and photoluminescence property of ZnO nanoparticles prepared by chemical precipitation method, *Acta Metall. Sin. (Engl. Lett.),* 2015, **28**, 394–404.

35 O. Garcia-Martinez, E. Vila, J.L. Martin de Vidales, R.M. Rojas and K. Petrov, On the thermal decomposition of the zinc(II) hydroxide chlorides Zn5(OH)8Cl2·H2O and β-Zn(OH)Cl, *J. Mater. Sci.,* 1994, **29**, 5429–5434.

36 S. Musić,Đ. Dragčević and S. Popović, Influence of synthesis route on the formation of ZnO particles and their morphologies, *J. Alloy. Comp.,* 2007, **429**, 242–249.

37 S.S. Kurbanov, G.N. Panin, T.W. Kim and T.W. Kang, Strong violet luminescence from ZnO nanocrystals grown by the low-temperature chemical solution deposition, *J. Lumin.,* 2009, **129**, 1009–1104.

38 M.K. Patra, K. Manzoor, M. Manoth, S.R. Vadera and N. Kumar, Studies of luminescence properties of ZnO and ZnO:Zn nanorods prepared by solution growth technique, *J. Lumin.,* 2008, **128**, 267–272.

39 J. Yang, R.Wang, L. Yang, J. Lang and N. Yang, Tunable deep-level emission in ZnO nanoparticles via yttrium doping, *J. Alloy. Comp.,* 2011, **509**, 3606–3612.

40 L. Zhang, L. Yin, C. Wang, N. lun, Y. Qi and D. Xiang, Origin of visible photoluminescence of ZnO quantum dots: defect-dependent and size-dependent, *J. Phys. Chem. C,* 2010, **114**, 9651–9658.

41 H.M. Xiong, D.G. Shchukin, H. Mohwald, Y. Xu and Y.Y. Xia, Sonochemical synthesis of highly luminescent zinc oxide nanoparticles doped with magnesium (II), *Angew. Chem., Int. Ed.,* 2009, **48**, 2727–2731.

42 W. Mingsong, N.K. Eun, K.S. Jae, K. J. Eui and K. Kee-Kahb, Photoluminescence of ZnO nanoparticles prepared by a low- temperature colloidal chemistry method, *Mater. Lett.,* 2007, **61**, 4094–4096.

43 N.R. Thimmasandra and L.M. Theeta, Thermal decomposition studies of layered metal hydroxynitrates (metal: Cu, Zn, Cu/Co, and Zn/Co), *Int. J. Inorg. Chem.,* 2015, Article ID 536470, http://dx.doi.org/10.1155/2015/536470

44 A. Jean-Paul and L. Daniel, Etude thermodynamique de la décomposition thermique des hydroxynitrates de zinc, *J. Solid State Chem.,* 1983, **46**, 245–252.

45 B. Timothy, J. William, P. Alexandra, S. Ewa and P. Jerzy, The role of anhydrous zinc nitrate in the thermal decomposition of the zinc hydroxy nitrates Zn5(OH)8(NO3)2.2H2O and ZnOHNO3.H2O, *J. Solid State Chem.,* 2007, **180**, 1171–1179.

46 J. Sithole, B.D. Ngom, S. Khamlich, E. Manikanadan, N. Manyala, M.L. Saboungi, D. Knoessen, R. Nemutudi and M. Maaza, Simonkolleite nano-platelets: synthesis and temperature effect on hydrogen gas sensing properties, *Appl. Surf. Sci.,* 2012, **258**, 7839–7843.

47 L. Tengfa, Y. Shu, T. Kouta T, Z. Peilin and S. Tsugio, Synthesis and characterization of ZnO nanorods and nanodisks from zinc chloride aqueous solution, *Nanoscale Res. Lett.*, 2009, **4**, 247–253.

48 H.B.Z. Mohd, G.Y. Mohammad, Y.H. Asmah and R.A.Z. Mohd, The effect of polymers onto the size of zinc layered hydroxide salt and its calcined product, *Solid State Sci.*, 2009, **11**, 368–375.

49 Z.P. Xu and H.C. Zeng, Ionic interactions in crystallite growth of CoMgAl-hydrotalcite-like compounds, *Chem. Mater.*, 2001, **13**, 4555–4563.

50 P. Chat, S. Chitnarong and J. H. David, Characterizations of octahedral zinc oxide synthesized by sonochemical method, *J. Phys. Chem. Solids*, 2011, **72**, 817–823.